Received 21 June 2020; accepted 9 July 2020. Date of publication 13 July 2020; date of current version 30 July 2020.

Digital Object Identifier 10.1109/OJCOMS.2020.3008989

Full Field Radiant Flux Distribution of Multiple Tilted Flat Lambertian Light Sources

JUAN CAMILO VALENCIA-ESTRADA [1], BASTIEN BÉCHADERGUE [1], AND JORGE GARCÍA-MÁRQUEZ [2]

[1]Research and Development Department, Oledcomm, 78140 Vélizy-Villacoublay, France

[2]Pôle Photonique—Energétique, Laboratoire National de Métrologie et d'Essais, 78190 Trappes, France

CORRESPONDING AUTHOR: B. BÉCHADERGUE (e-mail: bastien.bechadergue@oledcomm.net)

This work was supported by the European Union's Horizon 2020 Research and Innovation Programme under Grant 761992 (IoRL).

This article has supplementary downloadable material available at http://ieeexplore.ieee.org, provided by the authors.

ABSTRACT The emergence of visible light communication (VLC) as a subset of optical wireless communication (OWC) in the early 2000s has turned any light-emitting diode (LED) source into a potential data transmitter. The design process for any VLC or OWC system typically involves a link budget analysis performed by studying the signal-to-noise ratio (SNR) at the receiver. Since this SNR strongly depends on the radiant flux collected by the receiver, an accurate model for this parameter is required. The point-source model has been widely used since 1979 and generally provides a good approximation of the received radiant flux. However, it might be less accurate for typical extended lighting sources like LED panels or large-area organic LEDs. In this paper, the radiant flux distribution of flat Lambertian rectangular or circular sources is derived from a vector analysis of their irradiance. It is then validated through actual measurements in the case of a circular source. The resulting extended-source models thus better capture the light beam pattern of such transmitters to enable a more accurate link budget. It provides at the same time almost identical results to the point-source model for small sources and can, therefore, be seen as a natural extension of this already widely used model.

INDEX TERMS LED pattern, irradiance pattern, light power pattern, non-imaging optics, link budget, optical wireless communication, visible light communication.

I. INTRODUCTION

OPTICAL wireless communications (OWC) have been investigated since the 1960s for various applications ranging from high-speed point-to-point communication over long distances to optical camera communication or indoor networking [1]–[4]. This research has increased significantly since the 2000s, following the market introduction of white light-emitting diodes (LED) that can turn any lighting into a potential visible light communication (VLC) system [5], [6]. The concept of Light-Fidelity (LiFi), although already studied since the 1970s [1], has then been recently formalized to enable user devices networking through light [7], [8].

The first step in designing any OWC system needs a link budget analysis. The purpose is to estimate the value of the signal-to-noise ratio (SNR) at the receiver level in different situations. From this SNR, the quality of the communication link - its error rate for a given data rate, for example - can then be determined, which in turn allows specific critical system parameters to be adjusted. The SNR is not only highly dependent on the communication distance but also the link geometry and the parameters of the transmitting light source and the receiver. In particular, one of the key parameters is the radiant flux, collected by the receiver, which is directly proportional to the number of photons impinging on the photoreceiver, and whose increase is often synonymous with better performance. Note that the radiant flux is also often called optical power, especially in the OWC community.

In their 1979 article [1], Gfeller and Bapst proposed a model of the optical wireless channel that allows the average radiant flux collected by the receiver to be evaluated from the average radiant flux radiated by the light source. This model takes into account many parameters, such as the communication distance, the emission and reception angles, the surface and the sensitivity of the receiver, and it allows

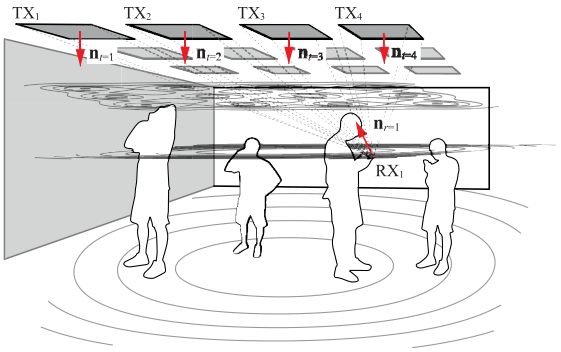

FIGURE 1. Illustration of a typical OWC use case with square panel light transmitters that can be addressed more accurately with the proposed model.

the effect of optical concentrators to be included [2]. It also allows taking into account not only the direct line-of-sight (LOS) rays but also the non-LOS (NLOS) rays that arrive on the receiver surface after one or more reflections. This first model has thus been successfully used in numerous subsequent works so that it is now widely prescribed as the standard OWC channel model [8]–[10]. At the same time, it has been improved to allow faster simulations, for example, using stochastic methods [11]–[13].

However, this model is based on the assumption that the light source is a point source whose transmission pattern follows a generalized Lambert's cosine law. While such an assumption is somewhat relevant when considering a simple LED chip, it may be more limited for extended sources. However, the emergence of VLC shows that wide-area light sources such as LED panels or even organic LEDs (OLED) can be used as emitters. In such cases, a more suitable model is therefore required. In [14], Moreno proposed a model of the irradiance of extended light sources and validated its relevance by comparing it with irradiance readings of real LEDs. This model is, however, only given in the case of a receiver whose sensitive surface is parallel to the emission surface of the transmitter.

In this article, we propose to extend this model to the case of multiple light sources and receivers tilted independently of each other, as illustrated by Fig. 1. For this purpose, we use a vector analysis of the irradiance of a transmitter that is initially not tilted and then introduce a change of the Cartesian coordinate system to take into account the tilt angle. Concerning the *mise en pratique* for the definition of the candela and other derived quantities, we refer to the International System (SI) units [15], while a valuable treaty on optical radiation, and specially radiance, exitance and irradiance can be found in [16]. From the resulting irradiance expression, we can then easily derive the radiant flux received by the receiver and thus end up with a flexible model that is more accurate than the point model for establishing link budgets. We verify at the same time that our model matches the point-source model in the case of small area transmitters, and establish a few orders of magnitude to define which model should be used according to the link geometry. The model proposed here can thus be seen as a natural extension of the point-source model already widely used. Finally, we validate the proposed model for circular sources through measurements of the radiant flux produced by a real source.

he rest of this article is organized as follows. In Section II, we present the point-source model and the general assumptions underlying our developments. Section III then details the calculation of the collected radiant flux in the case of a single non-tilted transmitter and tilted receiver. Section IV shows how to take into account the light source tilt and then how to take into account several independent transmitters. In Section V, the resulting model is compared to the point-source model in different configurations. Section VI then compares the theoretical model proposed for circular sources with actual measurements. Finally, Section VII draws some conclusions and relevant future works.

Notations: In this work, a vector $\mathbf{v}$ is denoted in bold font, whereas a scalar value x is denoted in regular font. The physical and geometrical parameters related to the transmitter and receiver are denoted with the subscripts t and r respectively. The notations $\bullet$, $\times$ and $\|.\|$ stand respectively for the vector product, the cross product and the vector norm in $\mathbb{R}^3$. $\mathscr{R} = (O, \mathbf{u}_x, \mathbf{u}_y, \mathbf{u}_z)$ is the Cartesian coordinate system of origin O and orthonormal basis defined by the vectors $\mathbf{u}_x$, $\mathbf{u}_y$ and $\mathbf{u}_z$. The coordinates x, y, and z of a point A in such a coordinate system are expressed $[x, y, z]_{\mathscr{R}}$. The rest of the notations and variable definitions are listed in Appendix A.

II. LIMITATIONS ADDRESSED AND GENERAL ASSUMPTIONS

A. THE POINT-LIKE SOURCE SCALAR APPROXIMATION

The communication performance of any OWC link strongly depends on the electrical SNR at the receiver level. This electrical SNR depends both on the modulation used and on the optical SNR. The latter, when expressed in the electrical domain, is defined as the ratio between the power of the photocurrent output by the photoreceiver and the power N_r of the noise in this photocurrent, that is [2]:

$$\mathrm{SNR} = \frac{R_r^2 \Phi_r^2}{N_r}, \tag{1}$$

with R_r the responsivity pattern of the receiver and Φ_r the average radiant flux collected by the receiver. Any link budget analysis based on the SNR thus relies on the accurate estimation of this radiant flux Φ_r, which depends on the properties of the light source and receiver as well as on their relative position and orientation.

In practice, several methods based on ray tracing have been proposed to simulate Φ_r according to the link configuration. Whether they are deterministic [1], [2], [9], or stochastic [11]–[13], they generally consider the received radiant flux to be the sum of the LOS contributions and NLOS contributions coming from reflections. Fig. 2 shows a typical LOS link geometry. The coordinate system takes as origin the center of the light source, which emits a light beam with an azimuth angle θ_t and a polar angle ϕ_t, defined according to the mathematical convention. This beam impinges on

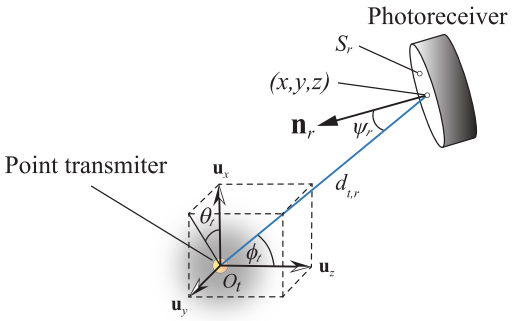

FIGURE 2. Illustration of a LOS link geometry with a point source. With a point-like transmitter, any axis of reference can be selected. However, we assume here that the $\mathbf{u}_z$ axis is the reference or main axis, because the transmitters are usually fixed to a horizontal ceiling with no tilt.

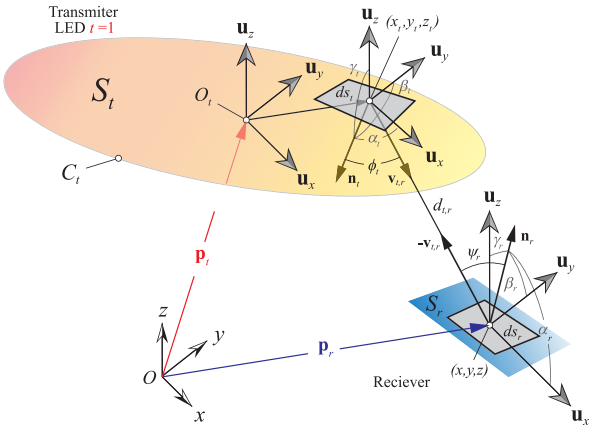

FIGURE 3. Differential model used to calculate the radiation pattern of an extended light source.

the receiver sensitive area S_r with an incidence angle ψ_r compared to its normal. Note that if this incidence angle is larger than the field-of-view (FOV) Ψ_r of the receiver, then the light beam will not be collected.

Following the work of Gfeller and Bapst in 1979 [1], the light source is considered as a point source rather than as an extended source and has an intensity $I_t(\theta_t, \phi_t)$, in W.sr^{-1}, expressed as:

$$I_t(\theta_t, \phi_t) = \Phi_t R_t(\theta_t, \phi_t). \tag{2}$$

where Φ_t is the average radiant flux emitted by the transmitter, and $R_t(\theta_t, \phi_t)$ is its radiation pattern. Note that the correct use of intensity is explained in [17]. This radiation pattern is then usually assumed to follow a generalized Lambertian cosine law, which is symmetrical about its reference axis so that:

$$R_t(\theta_t, \phi_t) = R_t(\phi_t) = \frac{m_t + 1}{2\pi} \cos^{m_t} \phi_t, \tag{3}$$

where m_t is the Lambertian order of the light source, related to its semi-angle at half power $\Phi_{t,1/2}$ by $m_t = -\ln 2 / \ln(\cos \Phi_{t,1/2})$ [18]. From the resulting expression of the intensity, it is possible to deduce the irradiance $E_{r,\,\text{point}}$ at the receiver level using the relation $E_{r,\,\text{point}} = I_t/d_{t,r}^2$, with $d_{t,r}$ the distance between the transmitter and the point at which the irradiance is calculated. Finally, the radiant flux collected by the receiver $\Phi_{r,\,\text{point}}$ can be calculated, assuming the irradiance is uniform over its surface S_r using $\Phi_{r,\,\text{point}} \approx S_r E_{r,\,\text{point}}$. Then, with (2) and (3), and assuming no optical filter and concentrator are used, we can derive a relation between Φ_t and Φ_r of the form [2]:

$$\Phi_{r,\,\text{point}} = H(0)\Phi_t. \tag{4}$$

with $H(0)$ the LOS channel DC gain, defined as:

$$H(0) = \begin{cases} \frac{(m_t+1)S_r}{2\pi d_{t,r}^2} \cos^{m_t} \phi_t \cos \psi_r & \text{if } \begin{array}{l} 0 \le \psi_r \le \Psi_r, \\ 0 \le \phi_t \le \pi/2, \end{array} \\ 0 & \text{otherwise.} \end{cases} \tag{5}$$

This model has been widely used in a vast majority of simulation works on OWC, as it provides an overall reliable estimate of the radiant flux collected for a little computational cost, with high scalability and flexibility. For example, several transmitters can easily be simulated at the same time by adding their respective contributions. The use of a single coordinate system for all transmitters and receivers is the only requirement. However, this model relies on the strong assumption that the light source is a point source. This assumption can be relevant when considering a simple LED chip, which is in practice the usual kind of transmitter used in infrared OWC systems.

However, the use of conventional LED lights as data transmitters has been studied since the 2000s and the emergence of the VLC [5], [6]. These LED lights can take several forms, for example 600×600 mm panels diffusing the light of a single LED chip or long linear tubes. The recent emergence of OLED also shows that lighting sources can take very wide-area and flexible forms. In such cases, the point source assumption may be more limited.

Moreover, the deployment of these lights is highly dependent on the shape of the space to be equipped. Consequently, not all sources may be arranged in the same plane and especially with the same tilt. Taking into account these different tilts in (5) usually requires a change of reference coordinates or the addition of tilt angles, which is not straightforward. The next sections will detail the simple model proposed to better take into account these realities.

B. LINK GEOMETRY STUDIED AND METHODOLOGY

The model proposed in this paper has been derived using a vector analysis carried out in a fixed Cartesian coordinate system $\mathscr{R} = (O_t, \mathbf{u}_x, \mathbf{u}_y, \mathbf{u}_z)$. Fig. 3 represents the link geometry considered, which includes the differential element ds_t of a light source of surface S_t, and the differential element ds_r of a receiver of surface S_r, along with the various geometrical parameters defining their relative position. Note that by convention, we will consider that the z-axis is defined by the unit vector $\mathbf{u}_z$ pointing toward the ceiling of the set-up.

Both differential elements have an associated normal unit vector, $\mathbf{n}_t$ and $\mathbf{n}_r$, respectively, which shows their orientations in the $\mathbb{R}^3$ space. Their coordinates are defined by the Euler's angles, α_t, β_t, γ_t, and α_r, β_r, γ_r respectively, between their normal vector and the coordinates axis as follows:

$$\begin{cases} \mathbf{n}_t = \left[\cos\alpha_t, \cos\beta_t, \cos\gamma_t\right] = [a_t, b_t, c_t]_{\mathscr{R}}, \\ \mathbf{n}_r = \left[\cos\alpha_r, \cos\beta_r, \cos\gamma_r\right] = [a_r, b_r, c_r]_{\mathscr{R}}. \end{cases} \tag{6}$$

The light ray generated by the point of coordinates $[x_t, y_t, z_t]_{\mathscr{R}}$ on the light source and impinging on the receiver at the $[x, y, z]_{\mathscr{R}}$ coordinate point has a direction defined by the unit vector $\mathbf{v}_{t,r}$ and travels a distance $d_{t,r}$. The angle of emission ϕ_t is defined as the angle between $\mathbf{n}_t$ and $\mathbf{v}_{t,r}$, whereas the angle of incidence ψ_r is the angle between $\mathbf{n}_r$ and $-\mathbf{v}_{t,r}$.

Our analysis is based on the source irradiance. The irradiance E_r is the radiant flux, or power, of a light source received by a surface per unit area, and is expressed in W.m^{-2}. Note that the irradiance E_r is thus different from the radiant exitance M_t of a transmitter, which is the radiant flux emitted per unit area of this transmitter and is also expressed in W.m^{-2}. In practice, E_r depends on the position $[x, y, z]_{\mathscr{R}}$ of the point at which it is calculated, as well as on the normal $\mathbf{n}_r$ of the surface to which this point belongs. It also depends on the orientation of the light source itself, defined by $\mathbf{n}_t$. Therefore, the irradiance could be noted $E_r(x, y, z, \mathbf{n}_t, \mathbf{n}_r)$, but we will use the lighter notation E_r instead for ease of reading. The irradiance can be calculated by integrating the transmitter radiance L_t, expressed in W.m^{-2}.sr^{-1}, over the source area S_t [19]:

$$E_r = \iint_{S_t} \frac{L_t \cos\phi_t \cos\psi_r}{d_{t,r}^2} ds_t. \tag{7}$$

Then, the total radiant flux on the receiver can be calculated by integrating the irradiance over the receiver surface using:

$$\Phi_r = \iint_{S_r} E_r \, ds_r, \tag{8}$$

In this paper, we only consider Lambertian light sources. A Lambertian source has, by definition, a constant radiance L_t, which can be linked to its average radiant flux Φ_t and its surface S_t by [19]:

$$L_t = \frac{\Phi_t}{\pi S_t}. \tag{9}$$

Note that a Lambertian source thus corresponds to a source with Lambertian order $m_t = 1$. Besides, we consider these Lambertian sources to be planar and either rectangular with sides $w_t \times h_t$, or circular with diameter d_t. Given these general assumptions, the main challenge is to derive the irradiance expression of such an extended source.

III. MODEL FOR A NON-TILTED LIGHT SOURCE AND A TILTED RECEIVER

A. GENERAL EXPRESSION OF IRRADIANCE FOR A PLANAR SOURCE

Let a planar Lambertian light source of surface S_t and contour C_t, fixed to a horizontal ceiling with no tilt. Let $\mathscr{R} = (O_t, \mathbf{u}_x, \mathbf{u}_y, \mathbf{u}_z)$ be the Cartesian coordinate system with O_t located at the center of the transmitter, $\mathbf{u}_x$ and $\mathbf{u}_y$ contained in the ceiling plane, and $\mathbf{u}_z$ pointing outside the room. As the transmitter is not tilted, we have $\mathbf{n}_t = -\mathbf{u}_z = [0, 0, -1]_{\mathscr{R}}$. The irradiance E_r of such a transmitter in a surface of coordinates $[x, y, z]_{\mathscr{R}}$ and unit normal vector $\mathbf{n}_r = [a_r, b_r, c_r]_{\mathscr{R}}$ is then given by:

$$E_r = L_t \left(\int_{C_t} \frac{-b_r z + c_r (y - y_t)}{2\left((x - x_t)^2 + (y - y_t)^2 + z^2\right)} dx_t + \int_{C_t} \frac{a_r z - c_r (x - x_t)}{2\left((x - x_t)^2 + (y - y_t)^2 + z^2\right)} dy_t \right). \tag{10}$$

Proof: As represented in Fig. 3, ϕ_t is the angle between the normal of the differential element of light source $\mathbf{n}_t = [a_t, b_t, c_t]_{\mathscr{R}}$ and the direction of emission of the light ray that goes from this differential element of the light source to the differential element of the receiver. This direction of emission is materialized by the unit vector $\mathbf{v}_{t,r} = [(x - x_t)/d_{t,r}, (y - y_t)/d_{t,r}, (z - z_t)/d_{t,r}]_{\mathscr{R}}$. Therefore, $\cos\phi_t$ can be retrieved from the scalar product between $\mathbf{n}_t$ and $\mathbf{v}_{t,r}$, that is:

$$\begin{aligned} \cos\phi_t &= \mathbf{v}_{t,r} \bullet \mathbf{n}_t \\ &= \frac{a_t(x - x_t) + b_t(y - y_t) + c_t(z - z_t)}{d_{t,r}} \\ &= \frac{a_t(x - x_t) + b_t(y - y_t) + c_t(z - z_t)}{\sqrt{(x - x_t)^2 + (y - y_t)^2 + (z - z_t)^2}}. \end{aligned} \tag{11}$$

Similarly, ψ_r is the angle between the normal of the differential element of receiver $\mathbf{n}_r = [a_r, b_r, c_r]_{\mathscr{R}}$ and the direction of reception of the light ray, materialized by the unit vector $-\mathbf{v}_{t,r}$, and can thus be retrieved from the scalar product between $\mathbf{n}_r$ and $-\mathbf{v}_{t,r}$, that is:

$$\begin{aligned} \cos\psi_r &= -\mathbf{v}_{t,r} \bullet \mathbf{n}_r \\ &= -\frac{a_r(x - x_t) + b_r(y - y_t) + c_r(z - z_t)}{d_{t,r}} \\ &= \frac{a_r(x_t - x) + b_r(y_t - y) + c_r(z_t - z)}{\sqrt{(x_t - x)^2 + (y_t - y)^2 + (z_t - z)^2}}. \end{aligned} \tag{12}$$

We assume the light source is planar and fixed with no tilt on a horizontal ceiling. Consequently, ds_t lies in the $(\mathbf{u}_x, \mathbf{u}_y)$ plane and its normal vector is $\mathbf{n}_t = [0, 0, -1]_{\mathscr{R}}$. Besides, we place the Cartesian coordinate origin in the middle of ds_t, which means $z_t = 0$. Therefore, (11) and (12) become:

$$\cos\phi_t = -\frac{z}{d_{t,r}}, \tag{13}$$

$$\cos\psi_r = -\frac{a_r(x - x_t) + b_r(y - y_t) + c_r z}{d_{t,r}}. \tag{14}$$

Using (13) and (14) in (7) and then simplifying, we obtain:

$$E_r = \iint_{S_t} \frac{L_t z (a_r(x - x_t) + b_r(y - y_t) + c_r z)}{\left((x - x_t)^2 + (y - y_t)^2 + z^2\right)^2} dx_t dy_t. \tag{15}$$

We assume now the light source has a Lambertian emission pattern, i.e., its radiance L_t is constant across locations on the transmitter surface. In this case, the integral in (15) has analytical solutions which can be obtained either by direct integration or by changing the surface integral into a contour integral in an $\mathbb{R}^3$ space by applying the Stokes theorem [14], [20]. Here, we present the contour's integral method as we consider the integration conditions make the procedure simpler.

According to the usual definition of the integral theorem of Stokes [21], if a vector field $\mathbf{F} = [P(x, y, z), Q(x, y, z), R(x, y, z)]_{\mathscr{R}}$ is defined in a region with smooth oriented surface Σ and has first-order continuous partial derivatives, then:

$$\iint_{\Sigma}\left(\frac{\partial R}{\partial y}-\frac{\partial Q}{\partial z}\right)dydz+\left(\frac{\partial P}{\partial z}-\frac{\partial R}{\partial x}\right)dzdx + \left(\frac{\partial Q}{\partial x}-\frac{\partial P}{\partial y}\right)dxdy=\int_{\partial\Sigma}(Pdx+Qdy+Rdz). \quad (16)$$

where P, Q, and R are the components of $\mathbf{F}$, and $\partial\Sigma$ is the boundary of the region with smooth surface Σ. Here, the planar light source of surface $\Sigma = S_t$ is contained in the $(\mathbf{u}_x, \mathbf{u}_y)$ plane, so $dz = 0$. As a consequence, the integral theorem of Stokes becomes Green's theorem which, applied to our case, states that:

$$\iint_{S_t}\left(\frac{\partial Q}{\partial x_t}-\frac{\partial P}{\partial y_t}\right)dx_t dy_t=\int_{C_t}(Pdx_t+Qdy_t), \quad (17)$$

where C_t is the contour of the light source surface S_t.

We notice the left term of (17) and (15) have the same form, so we simply have to find the expressions of P and Q to transform (15) into a contour integral. By following the method described in [20, Ch. 4, p. 182] with $dz = 0$ and $z_t = 0$, we find that:

$$P=\frac{-b_r z+c_r(y-y_t)}{2\left((x-x_t)^2+(y-y_t)^2+z^2\right)}, \quad (18)$$

$$Q=\frac{a_r z-c_r(x-x_t)}{2\left((x-x_t)^2+(y-y_t)^2+z^2\right)}. \quad (19)$$

We can easily verify with (18) and (19) that $\partial Q/\partial x_t - \partial P/\partial y_t = z(a_r(x-x_t)+b_r(y-y_t)+c_r z)/d_{t,r}^2$. Then, using these equations, we can transform (15) into the contour integral given in (10). ■

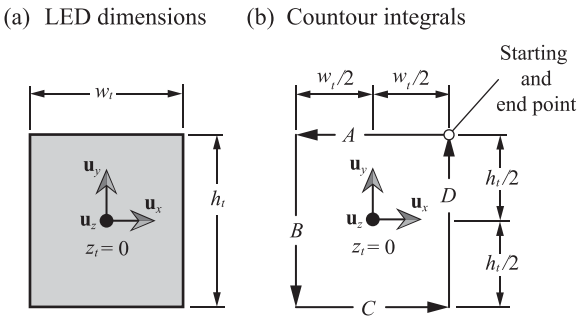

FIGURE 4. Rectangular light source dimensions and its contour integration. The contour integral is represented from the point of view of an observer in the $z > 0$ half-space looking at an irradiance pattern located in the $z < 0$ half-space.

B. CASE OF A PLANAR RECTANGULAR LIGHT SOURCE

We can derive from (10) the irradiance produced by different kinds of light sources. Here, we consider a rectangular light source of sides $w_t \times h_t$, as represented in Fig. 4(a). In this case, and under the same assumptions as in Section III-A, the irradiance $E_{r,\,\mathrm{rect}}$ impinging on a photoreceiver located in $[x, y, z]_{\mathscr{R}}$, with $z < 0$, and of normal vector $\mathbf{n}_r = [a_r, b_r, c_r]_{\mathscr{R}}$ is given by (20), as shown at the bottom of the page, and null if $z > 0$.

Proof: Equation (20) can be obtained by evaluating (10) following the rectangular contour C_t of the light source of sides $w_t \times h_t$. This contour can be followed clockwise or counterclockwise. However, it is better to follow it with the tip of the normal vector to the left. Thus, for an observer in the $z > 0$ domain, the contour integral is counterclockwise, while for an observer in the $z < 0$ domain, the contour integral is clockwise. Here, we assume $z > 0$ so that the contour is followed counterclockwise, as shown in Fig. 4(b). Equation (10) thus becomes the sum of four integrals, A, B, C, and D, each corresponding to one side of the rectangular source:

$$E_{r,\,\mathrm{rect}}=\frac{L_t}{2}(A+B+C+D), \quad (21)$$

$$\begin{aligned}E_{r,\,\mathrm{rect}}=\frac{\Phi_t}{2\pi w_t h_t}&\left(\frac{b_r z-c_r(y-h_t/2)}{\sqrt{(y-h_t/2)^2+z^2}}\left(\tan^{-1}\left(\frac{x+w_t/2}{\sqrt{(y-h_t/2)^2+z^2}}\right)-\tan^{-1}\left(\frac{x-w_t/2}{\sqrt{(y-h_t/2)^2+z^2}}\right)\right)\right.\\&+\frac{a_r z-c_r(x+w_t/2)}{\sqrt{(x+w_t/2)^2+z^2}}\left(\tan^{-1}\left(\frac{y-h_t/2}{\sqrt{(x+w_t/2)^2+z^2}}\right)-\tan^{-1}\left(\frac{y+h_t/2}{\sqrt{(x+w_t/2)^2+z^2}}\right)\right)\\&+\frac{b_r z-c_r(y+h_t/2)}{\sqrt{(y+h_t/2)^2+z^2}}\left(\tan^{-1}\left(\frac{x-w_t/2}{\sqrt{(y+h_t/2)^2+z^2}}\right)-\tan^{-1}\left(\frac{x+w_t/2}{\sqrt{(y+h_t/2)^2+z^2}}\right)\right)\\&\left.+\frac{a_r z-c_r(x-w_t/2)}{\sqrt{(x-w_t/2)^2+z^2}}\left(\tan^{-1}\left(\frac{y+h_t/2}{\sqrt{(x-w_t/2)^2+z^2}}\right)-\tan^{-1}\left(\frac{y-h_t/2}{\sqrt{(x-w_t/2)^2+z^2}}\right)\right)\right)\end{aligned} \quad (20)$$

with the contour integrals:

$$\begin{cases} A = \int_{w_t/2}^{-w_t/2} \frac{-b_r z + c_r(y - y_t)}{(x-x_t)^2+(y-y_t)^2+z^2}\Big|_{y_t=h_t/2} dx_t, \\ B = \int_{h_t/2}^{-h_t/2} \frac{a_r z - c_r(x - x_t)}{(x-x_t)^2+(y-y_t)^2+z^2}\Big|_{x_t=-w_t/2} dy_t, \\ C = \int_{-w_t/2}^{w_t/2} \frac{-b_r z + c_r(y - y_t)}{(x-x_t)^2+(y-y_t)^2+z^2}\Big|_{y_t=-h_t/2} dx_t, \\ D = \int_{-h_t/2}^{h_t/2} \frac{a_r z - c_r(x - x_t)}{(x-x_t)^2+(y-y_t)^2+z^2}\Big|_{x_t=w_t/2} dy_t, \end{cases} \tag{22}$$

that, once evaluated, become:

$$\begin{cases} A = \int_{w_t/2}^{-w_t/2} \frac{-b_r z + c_r(y - h_t/2)}{(x-x_t)^2+(y-h_t/2)^2+z^2} dx_t, \\ B = \int_{h_t/2}^{-h_t/2} \frac{a_r z - c_r(x + w_t/2)}{(x+w_t/2)^2+(y-y_t)^2+z^2} dy_t, \\ C = \int_{-w_t/2}^{w_t/2} \frac{-b_r z + c_r(y + h_t/2)}{(x-x_t)^2+(y+h_t/2)^2+z^2} dx_t, \\ D = \int_{-h_t/2}^{h_t/2} \frac{a_r z - c_r(x - w_t/2)}{(x-w_t/2)^2+(y-y_t)^2+z^2} dy_t. \end{cases} \tag{23}$$

Assuming that all the variables are real, the integrals in (23) can be derived and simplified to obtain:

$$\begin{cases} A = \frac{b_r z - c_r(y-h_t/2)}{\sqrt{(y-h_t/2)^2+z^2}}\left(\tan^{-1}\left(\frac{x+w_t/2}{\sqrt{(y-h_t/2)^2+z^2}}\right) - \tan^{-1}\left(\frac{x-w_t/2}{\sqrt{(y-h_t/2)^2+z^2}}\right)\right), \\ B = \frac{a_r z - c_r(x+w_t/2)}{\sqrt{(x+w_t/2)^2+z^2}}\left(\tan^{-1}\left(\frac{y-h_t/2}{\sqrt{(x+w_t/2)^2+z^2}}\right) - \tan^{-1}\left(\frac{y+h_t/2}{\sqrt{(x+w_t/2)^2+z^2}}\right)\right), \\ C = \frac{b_r z - c_r(y+h_t/2)}{\sqrt{(y+h_t/2)^2+z^2}}\left(\tan^{-1}\left(\frac{x-w_t/2}{\sqrt{(y+h_t/2)^2+z^2}}\right) - \tan^{-1}\left(\frac{x+w_t/2}{\sqrt{(y+h_t/2)^2+z^2}}\right)\right), \\ D = \frac{a_r z - c_r(x-w_t/2)}{\sqrt{(x-w_t/2)^2+z^2}}\left(\tan^{-1}\left(\frac{y+h_t/2}{\sqrt{(x-w_t/2)^2+z^2}}\right) - \tan^{-1}\left(\frac{y-h_t/2}{\sqrt{(x-w_t/2)^2+z^2}}\right)\right). \end{cases} \tag{24}$$

The set of equations (24) can then be inserted in (21) along with (9) to get (20). ■

It is important to mention that we can derive the solution proposed in [14] for a receiver placed at a vertical distance $z = -h$ from the transmitter and pointing toward the ceiling with a fixed orientation $\mathbf{n}_r = [0, 0, 1]_{\mathscr{R}}$ from (20).

The radiant flux collected by the receiver of area S_r can finally be evaluated by combining (8) with (20). The resulting integral only has an analytical solution by series. However, if the photoreceiver dimensions are small compared to the link distance $d_{t,r}$, then the irradiance $E_{r,\,\mathrm{rect}}(x, y, z)$ received in any point $[x, y, z]_{\mathscr{R}}$ on the photoreceiver surface can be assumed constant across this surface and equal to $\overline{E_r}$. Therefore, the next approximation is valid and allows to calculate easily $\Phi_{r,\,\mathrm{rect}}$:

$$\begin{aligned} \Phi_{r,\,\mathrm{rect}} &= \iint_{S_r} E_{r,\,\mathrm{rect}}(x, y, z)\ ds_r \\ &\approx \overline{E_{r,\,\mathrm{rect}}} \iint_{S_r} ds_r = S_r \overline{E_{r,\,\mathrm{rect}}}. \end{aligned} \tag{25}$$

C. CASE OF A PLANAR CIRCULAR LIGHT SOURCE

We consider now a circular light source of diameter d_t, as represented in Fig. 5(a). In this case, and under the same assumptions as in Section III-A, the irradiance $E_{r,\,\mathrm{circ}}$ impinging on a receiver located in $[x, y, z]_{\mathscr{R}}$, with $z < 0$, and of normal vector $\mathbf{n}_r = [a_r, b_r, c_r]_{\mathscr{R}}$ is given by:

$$E_{r,\,\mathrm{circ}} = \frac{2\Phi_t}{\pi d_t^2 \left(x^2 + y^2\right)}$$

(a) LED dimensions (b) Countour integral

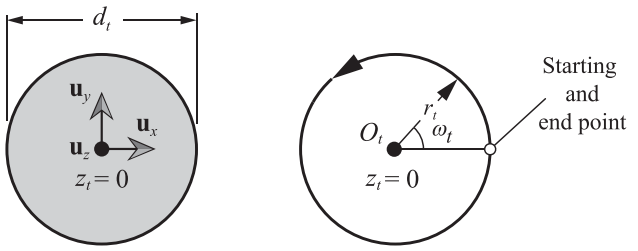

FIGURE 5. Circular source dimensions and contour integral. The contour integral is represented from the point of view of an observer in the $z > 0$ half-space looking at an irradiance pattern located in the $z < 0$ half-space.

$$\times \left[c_r\left(x^2 + y^2\right) - (a_r x + b_r y) z - \frac{c_r\left(x^2 + y^2\right)\left(4\left(x^2 + y^2 + z^2\right) - d_t^2\right)}{\sqrt{16 d_t^2 z^2 + \left(4\left(x^2 + y^2 + z^2\right) - d_t^2\right)^2}} + \frac{z(a_r x + b_r y)\left(4\left(x^2 + y^2 + z^2\right) + d_t^2\right)}{\sqrt{16 d_t^2 z^2 + \left(4\left(x^2 + y^2 + z^2\right) - d_t^2\right)^2}} \right]. \tag{26}$$

Proof: The irradiance of an extended circular transmitter of diameter d_t and radius $r_t = d_t/2$ can be derived from (10). To do this, it is first necessary to express the point-of-integration coordinates x_t and y_t on the light source contour and their differential dx_t and dy_t as functions of r_t. As the contour is here a circle, these Cartesian coordinates can also be expressed in polar coordinates according to the circle radius r_t and the polar angle ω_t, as represented in Fig. 5(b). Since r_t does not vary, then $dr_t = 0$. Therefore, the following change of variables can be introduced into (10):

$$\begin{cases} x_t \to r_t \cos\omega_t, \\ y_t \to r_t \sin\omega_t, \\ dx_t \to dr_t \cos\omega_t - r_t \sin\omega_t d\omega_t = -r_t \sin\omega_t d\omega_t, \\ dy_t \to dr_t \sin\omega_t + r_t \cos\omega_t d\omega_t = r_t \cos\omega_t d\omega_t, \end{cases} \tag{27}$$

After introducing this change of variables in (10) and simplifying, we get:

$$E_{r,\,\mathrm{circ}} = \frac{L_t}{2}\left[\int_{C_t} \frac{-r_t(c_r(x - r_t\cos\omega_t) - a_r z)\cos\omega_t}{(x - r_t\cos\omega_t)^2 + (y - r_t\sin\omega_t)^2 + z^2} d\omega_t - \int_{C_t} \frac{r_t(c_r(y - r_t\sin\omega_t) - b_r z)\sin\omega_t}{(x - r_t\cos\omega_t)^2 + (y - r_t\sin\omega_t)^2 + z^2} d\omega_t\right]. \tag{28}$$

The Cartesian integral is thus transformed into a polar integral, where the integration variable is the angle ω_t. As represented in Fig. 5(b), this angle varies between 0 and 2π to describe the full contour of the circular light source. Assuming all the variables are real and that $r_t > 0$, then the resulting integral has the following analytical solution:

$$E_{r,\,\mathrm{circ}} = \frac{L_t \pi \left(c_r\left(x^2 + y^2\right) - (a_r x + b_r y) z\right)}{2\left(x^2 + y^2\right)}$$

$$+\frac{A-B}{\sqrt{-16d_t^2z^2-\left(4\left(x^2+y^2+z^2\right)-d_t^2\right)^2}}\times\left[\frac{L_tc_r\left(x^2+y^2\right)\left(d_t^2-4\left(x^2+y^2+z^2\right)\right)}{2\left(x^2+y^2\right)}+\frac{L_tz(a_tx+b_ty)\left(d_t^2+4\left(x^2+y^2+z^2\right)\right)}{2\left(x^2+y^2\right)}\right], \tag{29}$$

where A and B are notations for:

$$\begin{cases} A=\log\left[\frac{-2\left((d_t+2x)^2+4\left(y^2+z^2\right)\right)}{\sqrt{-16d_t^2z^2-\left(4\left(x^2+y^2+z^2\right)-d_t^2\right)^2}}\right], \\ B=\log\left[\frac{2\left((d_t+2x)^2+4\left(y^2+z^2\right)\right)}{\sqrt{-16d_t^2z^2-\left(4\left(x^2+y^2+z^2\right)-d_t^2\right)^2}}\right]. \end{cases} \tag{30}$$

Let C and D be notations for:

$$\begin{cases} C=2\left((d_t+2x)^2+4\left(y^2+z^2\right)\right), \\ D=\sqrt{16d_t^2z^2+\left(4\left(x^2+y^2+z^2\right)-d_t^2\right)^2}. \end{cases} \tag{31}$$

The expression in the square root of D results from the addition of several squared real values and is thus always positive. Besides, as $d_t > 0$, this expression is always strictly positive. The expression in the square roots of the denominators of A and B is thus always negative, so that these square roots are imaginary and equal to iD, with i the imaginary number defined as $i^2 = -1$. From this observation, we can deduce that the second line in (29) is equal to $(A-B)/iD$ and that:

$$\frac{A-B}{iD}=\frac{\log\left[\frac{-C}{iD}\right]-\log\left[\frac{C}{iD}\right]}{iD}=\frac{\pi}{D}. \tag{32}$$

By introducing (32) and (9) into (29) and then simplifying, we can deduce the expression given in (26). ■

We can note that if the receiver is not tilted, that is if $\mathbf{n}_r = [0, 0, 1]_{\mathscr{R}}$, then (26) reduces into:

$$E_{r,\,\mathrm{circ}}=\frac{2\Phi_t}{\pi d_t^2}\left[1-\left(\frac{16d_t^2z^2}{\left(4\left(x^2+y^2+z^2\right)-d_t^2\right)^2}+1\right)^{-\frac{1}{2}}\right]. \tag{33}$$

Finally, we can note that the radiant flux $\Phi_{r,\,\mathrm{circ}}$ collected by the receiver of surface S_r can be obtained using (25) with (26) if we assume the received irradiance is constant across the photoreceiver surface.

IV. MODEL FOR MULTIPLE TILTED LIGHT SOURCES

A. GENERAL IRRADIANCE EXPRESSION WITH A LIGHT SOURCE TILT

We now consider the rectangular or circular planar transmitter of surface S_t is titled. As previously, let $\mathscr{R} = (O_t, \mathbf{u}_x, \mathbf{u}_y, \mathbf{u}_z)$ be the Cartesian coordinate system with O_t located at the center of the transmitter, $\mathbf{u}_x$ and $\mathbf{u}_y$ contained in the ceiling plane, and $\mathbf{u}_z$ pointing outside the room. As the transmitter is now tilted, we have $\mathbf{n}_t = [a_t, b_t, c_t]_{\mathscr{R}}$ with $\mathrm{sign}(c_t) = -1$ and $c_t \neq -1$. In such a case, the irradiance E_r in a surface of coordinates $[x, y, z]_{\mathscr{R}}$ and unit normal vector $\mathbf{n}_r = [a_r, b_r, c_r]_{\mathscr{R}}$ can be obtained by changing, in (20) for rectangular sources or in (26) for circular sources, the variables x, y, z, a_r, b_r, and c_r by:

$$\begin{cases} x\to X, & X=-c_tx+a_tz+\frac{b_t(b_tx-a_ty)}{1-c_t}, \\ y\to Y, & Y=-c_ty+b_tz-\frac{a_t(b_tx-a_ty)}{1-c_t}, \\ z\to Z, & Z=-(a_tx+b_ty+c_tz), \end{cases} \tag{34}$$

and:

$$\begin{cases} a_r\to A_r, & A_r=-c_ta_r+a_tc_r+\frac{b_t(b_ta_r-a_tb_r)}{1-c_t}, \\ b_r\to B_r, & B_r=-c_tb_r+b_tc_r-\frac{a_t(b_ta_r-a_tb_r)}{1-c_t}, \\ c_r\to C_r, & C_r=-(a_ta_r+b_tb_r+c_tc_r). \end{cases} \tag{35}$$

Note that if $[a_t, b_t, c_t] = [0, 0, -1]$ then $x = X$, $y = Y$ and $z = Z$, which means there is logically no change of variables needed.

Proof: Finding the transmitter pattern with tilt $\mathbf{n}_t = [a_t, b_t, c_t]_{\mathscr{R}}$, where $\mathrm{sign}(c_t) = -1$; $c_t \neq -1$, can be done either by control integral in $\mathbb{R}^3$ or by an axis rotation using Rodrigues formula [21]. The latter solution is considered here as it is most straightforward.

Let $\mathscr{R}' = (O, \mathbf{u}_X, \mathbf{u}_Y, \mathbf{u}_Z)$ be a coordinate system such that $\mathbf{u}_Z = -\mathbf{n}_t$, χ be the angle between $\mathbf{u}_z$ and $\mathbf{u}_Z$ and $\mathbf{k}$ be the unit director vector of the rotation of angle χ which transforms $\mathscr{R}$ into $\mathscr{R}'$. Fig. 6 shows an example of such coordinate systems, with $\mathbf{k} = \mathbf{u}_y$.

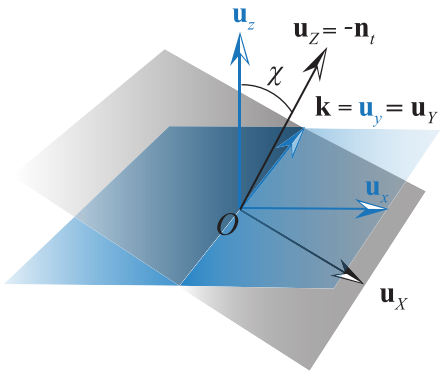

FIGURE 6. Example of coordinate system rotation applied to take the source tilt into account.

As demonstrated in Section III-B, the irradiance E_r at the point defined by the vector $\mathbf{v}_{t,r} = [x, y, z]_{\mathscr{R}}$ can be calculated for a rectangular transmitter using (20) and for a circular transmitter using (26) if the transmitter is not tilted, that is if $\mathbf{n}_t = [0, 0, -1]_{\mathscr{R}}$. Although the transmitter is here tilted in $\mathscr{R}$, it is not anymore in $\mathscr{R}'$ as $\mathbf{u}_Z = -\mathbf{n}_t$. Let X, Y, and Z be the coordinates of $\mathbf{v}_{t,r}$ in $\mathscr{R}'$. Then, the irradiance in $\mathbf{v}_{t,r}$ can simply be obtained using (20) with $\mathbf{v}_{t,r} = [X, Y, Z]_{\mathscr{R}'}$. Consequently, we now need to find the expressions of X, Y, and Z, according to x, y, and z. Since $\mathscr{R}$ and $\mathscr{R}'$ are both orthonormal basis, then:

$$\begin{cases} X=\mathbf{v}_{t,r}\bullet\mathbf{u}_X, \\ Y=\mathbf{v}_{t,r}\bullet\mathbf{u}_Y, \\ Z=\mathbf{v}_{t,r}\bullet\mathbf{u}_Z, \end{cases} \tag{36}$$

where all vectors are expressed in $\mathscr{R}$.

The problem is thus reduced to expressing the coordinates of the vectors $\mathbf{u}_X$, $\mathbf{u}_Y$, and $\mathbf{u}_Z$ in $\mathscr{R}$. We already know that $\mathbf{u}_Z = [-a_t, -b_t, -c_t]_{\mathscr{R}}$. Then, $\mathbf{u}_X$ and $\mathbf{u}_Y$ are respectively the images of $\mathbf{u}_x$ and $\mathbf{u}_y$ after rotation around the director vector $\mathbf{k}$ by an angle χ. According to Rodrigues formula, the image $\mathbf{u}'$ of a vector $\mathbf{u}$ after such rotation is:

$$\mathbf{u}' = \mathbf{u}\cos\chi + (\mathbf{k}\times\mathbf{u})\sin\chi + \mathbf{k}(\mathbf{k}\bullet\mathbf{u})(1-\cos\chi). \quad (37)$$

The first step in applying this formula is to determine the unit vector $\mathbf{k}$ acting as rotation pivot. $\mathbf{k}$ is a unit vector normal to the plane defined by $\mathbf{u}_z$ and $\mathbf{u}_Z$ and can thus be obtained using:

$$\mathbf{k} = \frac{\mathbf{u}_z \times \mathbf{u}_Z}{\|\mathbf{u}_z \times \mathbf{u}_Z\|}. \quad (38)$$

Here, with $\mathbf{u}_z = [0, 0, 1]_{\mathscr{R}}$ and $\mathbf{u}_Z = [-a_t, -b_t, -c_t]_{\mathscr{R}}$, and since $\|\mathbf{n}_t\|^2 = a_t^2 + b_t^2 + c_t^2 = 1$, we obtain:

$$\mathbf{k} = \left[\frac{b_t}{\sqrt{1-c_t^2}}, -\frac{a_t}{\sqrt{1-c_t^2}}, 0\right]_{\mathscr{R}}. \quad (39)$$

We also need to determine the rotation angle χ, which is the angle between $\mathbf{u}_z$ and $\mathbf{u}_Z$ that can be defined using the scalar product between these two vectors:

$$\cos\chi = \mathbf{u}_z \bullet \mathbf{u}_Z = -c_t \rightarrow \sin\chi = \sqrt{1-c_t^2}, \quad (40)$$

since $\cos^2\chi + \sin^2\chi = 1$.

We can now use (39), (40), $\mathbf{u}_x = [1, 0, 0]_{\mathscr{R}}$ and $\mathbf{u}_y = [0, 1, 0]_{\mathscr{R}}$ in (37) to conclude that:

$$\begin{cases} \mathbf{u}_X = \left[-c_t + \frac{b_t^2}{1-c_t}, -\frac{a_t b_t}{1-c_t}, a_t\right]_{\mathscr{R}}, \\ \mathbf{u}_Y = \left[-\frac{a_t b_t}{1-c_t}, -c_t + \frac{a_t^2}{1-c_t}, b_t\right]_{\mathscr{R}}, \\ \mathbf{u}_Z = [-a_t, -b_t, -c_t]_{\mathscr{R}}, \end{cases} \quad (41)$$

which, using (36), leads to the change of variables described in (35).

With these expressions of X, Y, and Z, we are now able to evaluate the irradiance at point $\mathbf{v}_{t,r}$ in $\mathscr{R}'$ using (20) for a rectangular source and (26) for a circular source. However, we must not forget that the coordinates a_r, b_r and c_r of the receiver normal $\mathbf{n}_r$ are set in $\mathscr{R}$ but not in $\mathscr{R}'$. In other words, $\mathbf{n}_r$ must also be rotated around $-\mathbf{k}$ by an angle $-\chi$ to obtain its coordinates A_r, B_r and C_r in $\mathscr{R}'$, which can be done using (41) in (36) with $\mathbf{v}_{t,r} = \mathbf{n}_r = [a_r, b_r, c_r]_{\mathscr{R}}$. It leads to the second change of variables described in (35). ■

It is important to mention that all formulas for the tilt free patterns are even functions, i.e., they are symmetric functions with respect to the $x-y$ plane, where one pattern is defined for the upper half of the plane $z > 0$, and the other for the lower half of the plane $z < 0$. When the tilt is performed, the plane that separates both patterns also rotates. For this reason, the condition that establishes the domain of each pattern can be expressed as $-(a_t x + b_t y + c_t z) > 0$ for all evaluation points $[x, y, z]_{\mathscr{R}}$ of the pattern on the positive semi-plane, and $-(a_t x + b_t y + a_t z) < 0$ for all evaluation points $[x, y, z]_{\mathscr{R}}$ of the pattern on the negative semi-plane.

B. EXTENSION TO SEVERAL POINT AND EXTENDED LIGHT SOURCES

It is often required to install several light sources in a given room. The previous results can be used to express, in a single Cartesian coordinate system $\mathscr{R}$, the irradiance pattern produced by these different light sources in an arbitrary point. This irradiance will depend on the position of each transmitter.

Assuming a total of T different transmitters, let $\mathbf{p}_t = [x_t, y_t, z_t]_{\mathscr{R}}$ be the position vector of the t-th transmitter, and $\mathbf{n}_t = [a_t, b_t, c_t]_{\mathscr{R}}$ be the unit vector describing its tilt. Then, assuming there is a receiver of normal vector $\mathbf{n}_r = [a_r, b_r, c_r]_{\mathscr{R}}$ at the point of coordinates $\mathbf{p}_r = [x, y, z]_{\mathscr{R}}$, the contribution E_r of this light source to the overall irradiance at that receiver level will be:

$$E_r = E_r(\mathbf{p}_r - \mathbf{p}_t, \mathbf{n}_t, \mathbf{n}_r), \quad (42)$$

and can be evaluated using (20) with the changes of variables (34) and (35) if the transmitter t is tilted.

The overall radiant flux $\Phi_{r,\,\text{total}}$ at that receiver level is then obtained by summation:

$$\Phi_{r,\,\text{total}} = \sum_{t=1}^{T} S_r E_r(\mathbf{p}_r - \mathbf{p}_t, \mathbf{n}_t, \mathbf{n}_r). \quad (43)$$

Note that if all the light sources are considered as point sources, then the resulting radiant flux distribution can be obtained by summing the contribution of each transmitter, calculated using (4) with $H(0)$ given by (5) where $d_{t,r}^2 = (x-x_t)^2 + (y-y_t)^2 + (z-z_t)^2$, $\cos\phi_t$ given by (11) and $\cos\psi_r$ given by (12).

V. COMPARISON BETWEEN THE MODELS

Now that the rectangular and circular-source models have been derived, we compare them with the point-source model. First, a mathematical analysis is detailed in Sections V-A and V-B to show that the three models are equivalent at large distance. Then, we focus in Sections V-C to V-E on the near-field behavior of the models through simulations.

A. THE POINT-LIKE SOURCE VECTOR APPROXIMATION

In order to study the behavior of the three models at large distances between the source and the photoreceiver, we first need to express the point-source model detailed in Section II in the Cartesian coordinate system used in Section III.

We consider here an OWC link as represented on Fig. 2 and composed of a non-tilted generalized Lambertian point source of Lambertian order m_t and of radiant flux Φ_t, and of a photoreceiver with FOV Ψ_r separated by a distance $d_{t,r}$. Let $\mathscr{R} = (O_t, \mathbf{u}_x, \mathbf{u}_y, \mathbf{u}_z)$ be the Cartesian coordinate system with O_t located at the center of the transmitter, $\mathbf{u}_x$ and $\mathbf{u}_y$ contained in the ceiling plane, and $\mathbf{u}_z$ pointing outside the room. As the transmitter is not tilted, we have $\mathbf{n}_t = -\mathbf{u}_z = [0, 0, -1]_{\mathscr{R}}$. On the other hand, we assume the center of the photoreceiver surface is located at the point of coordinates $[x, y, z]_{\mathscr{R}}$ and that this surface S_r has a unit normal vector

$\mathbf{n}_r = [a_r, b_r, c_r]_{\mathscr{R}}$. We also assume the received irradiance $E_{r,\,\text{point}}$ is constant across the photoreceiver surface so that $E_{r,\,\text{point}} = \Phi_{r,\,\text{point}}/S_r$. Then, if $z < 0$, the received irradiance $E_{r,\,\text{point}}$ is given by:

$$E_{r,\,\text{point}} = \frac{-\Phi_t(m_t+1)(-z)^{m_t}(a_r x + b_r y + c_r z)}{2\pi\left(x^2+y^2+z^2\right)^{(m_t+3)/2}}, \quad (44)$$

if:

$$\cos\Psi_r \leq \frac{-(a_r x + b_r y + c_r z)}{\sqrt{x^2+y^2+z^2}} \leq 1, \quad (45)$$

and null otherwise. If $z > 0$, $E_{r,\,\text{point}}$ is always null.

Proof: We already know from (4) and (5) that if the received irradiance is assumed constant across the photoreceiver surface, then:

$$\Phi_{r,\,\text{point}} = \begin{cases} \frac{\Phi_t(m_t+1)S_r}{2\pi d_{t,r}^2}\cos^{m_t}\phi_t \cos\psi_r & \text{if } \begin{matrix} 0 \leq \psi_r \leq \Psi_r, \\ 0 \leq \phi_t \leq \pi/2, \end{matrix} \\ 0 & \text{otherwise.} \end{cases} \quad (46)$$

This equation is valid only in the half-space of emission, that is if $z < 0$. Otherwise it is null. By dividing it by S_r, we can obtain the expression for the received irradiance $E_{r,\,\text{point}}$, that is:

$$E_{r,\,\text{point}} = \begin{cases} \frac{\Phi_t(m_t+1)}{2\pi d_{t,r}^2}\cos^{m_t}\phi_t \cos\psi_r & \text{if } \begin{matrix} 0 \leq \psi_r \leq \Psi_r, \\ 0 \leq \phi_t \leq \pi/2, \end{matrix} \\ 0 & \text{otherwise.} \end{cases} \quad (47)$$

Then, the goal is to express this equation in the coordinate system $\mathscr{R}$, which can be done by expressing $\cos\phi_t$ and $\cos\psi_r$ in $\mathscr{R}$ using (11) and (12). This gives:

$$\cos\phi_t = \mathbf{v}_{t,r} \bullet \mathbf{n}_t = \frac{-z}{\sqrt{x^2+y^2+z^2}}, \quad (48)$$

and:

$$\cos\psi_r - \mathbf{v}_{t,r} \bullet \mathbf{n}_r = \frac{-(a_r x + b_r y + c_r z)}{\sqrt{x^2+y^2+z^2}}. \quad (49)$$

Since $0 \leq \psi_r \leq \Psi_r$ and cos is an increasing function, we can deduce (45) from (49). Then, by combining (47), (48) at the power of m_t, and (49), we can obtain (44). ■

Note that in the case of a non-tilted photoreceiver with $\mathbf{n}_r = [0, 0, 1]_{\mathscr{R}}$, the radiant flux received (44) from a Lambertian point source ($m_t = 1$) becomes:

$$E_{r,\,\text{point}} = \frac{\Phi_t z^2}{\pi\left(x^2+y^2+z^2\right)^2} \quad (50)$$

B. COMPARATIVE ANALYSIS BETWEEN NON-TILTED MODELS

We can now compare mathematically the irradiance pattern collected with a non-tilted receiver from a Lambertian point source, a square source and a circular source using respectively (50), (20) with $h_t = w_t$, $a_r = b_r = 0$ and $c_r = 1$, and (33).

This irradiance comparison first requires a meridional asymptotic analysis. Therefore, we represent the rotationally symmetric irradiance patterns for the point-like and circular sources in cylindrical coordinates (ρ, z), through the change of variables $\{x^2+y^2 \to \rho\}$. The rectangular source irradiance pattern is not rotationally symmetric but has two orthogonal meridional sections: one of them contains the source's diagonal and has maximum irradiance, whereas the other contains either the x-axis or the y-axis and has minimum irradiance. In the case of a rectangular aperture source, it is of importance to consider meridional sections. However, we will use here the maximum irradiance case by taking into account the change of variables $\{x \to \rho\sqrt{2}/2, y \to \rho\sqrt{2}/2\}$.

To normalize (20) and (33) in such a way the square and circular sources areas are equal, we employ:

$$d_t = \frac{2w_t}{\sqrt{\pi}}. \quad (51)$$

In addition, we include a scale factor to measure the distances ρ and z with units w_t by posing $\hat{\rho} = \rho/w_t$ and $\hat{z} = z/w_t$. By fulfilling the considerations just described, we can represent the maximum irradiances in cylindrical coordinates for all three cases. In the case of the point-like source, we get:

$$E_{r,\,\text{point}} = \frac{\Phi_t \hat{z}^2}{\pi w_t^2\left(\hat{\rho}^2+\hat{z}^2\right)^2}, \quad (52)$$

In the case of a square source, we obtain:

$$E_{r,\,\text{square}} = \frac{\Phi_t}{\pi w_t^2}\Big(A\Big(\tan^{-1}A - \tan^{-1}B\Big) + C\Big(\tan^{-1}C - \tan^{-1}D\Big)\Big). \quad (53)$$

with:

$$\begin{cases} A = \frac{\sqrt{2}\hat{\rho}-1}{\sqrt{\left(\sqrt{2}\hat{\rho}-1\right)^2+4\hat{z}^2}}, \\ B = \frac{\sqrt{2}\hat{\rho}+1}{\sqrt{\left(\sqrt{2}\hat{\rho}-1\right)^2+4\hat{z}^2}}, \\ C = \frac{\sqrt{2}\hat{\rho}+1}{\sqrt{\left(\sqrt{2}\hat{\rho}+1\right)^2+4\hat{z}^2}}, \\ D = \frac{\sqrt{2}\hat{\rho}-1}{\sqrt{\left(\sqrt{2}\hat{\rho}+1\right)^2+4\hat{z}^2}}. \end{cases} \quad (54)$$

Finally, in the case of a circular source, we get:

$$E_{r,\,\text{circ}} = \frac{\Phi_t}{2w_t^2}\left[1 - \left(1 + \pi\left(\frac{2\hat{z}}{\pi\left(\hat{\rho}^2+\hat{z}^2\right)-1}\right)^2\right)^{-1/2}\right]. \quad (55)$$

This new set of equations allows to compute the ratios $\frac{E_{r,\,\text{point}}}{E_{r,\,\text{square}}}$ and $\frac{E_{r,\,\text{point}}}{E_{r,\,\text{circ}}}$ and to study their limit when the distance between the source and the photoreceiver increases. It is worth mentioning that the normalized ratios do not depend on the radiant flux Φ_t nor the source's dimension w_t.

In order to focus our study on the maximum irradiance provided by each of the three models, we now assume the

photoreceiver is in the axis of the source, that is $\hat{\rho} = 0$. Then, we can show that:

$$\lim_{\hat{z}\to\pm\infty} \frac{E_{r,\text{ point}}}{E_{r,\text{ square}}} = 1, \tag{56}$$

and:

$$\lim_{\hat{z}\to\pm\infty} \frac{E_{r,\text{ point}}}{E_{r,\text{ circ}}} = 1. \tag{57}$$

These results show that the proposed extended-source models are equivalent to the point-source model at large distance.

Proof: Since $\hat{\rho} = 0$, then (52), (53), (54) become respectively:

$$E_{r,\text{ point}} = \frac{\Phi_t}{\pi w_t^2 \hat{z}^2}, \tag{58}$$

$$E_{r,\text{ square}} = \frac{2\Phi_t}{\pi w_t^2 \left(1+4\hat{z}^2\right)}\left[\tan^{-1}\frac{1}{1+4\hat{z}^2} - \tan^{-1}\frac{-1}{1+4\hat{z}^2}\right], \tag{59}$$

and:

$$E_{r,\text{ circ}} = \frac{\Phi_t}{2w_t^2}\left[1 - \left(1+\pi\left(\frac{2\hat{z}}{\pi\hat{z}^2-1}\right)^2\right)^{-1/2}\right], \tag{60}$$

In the case of the square source, we can see that $\frac{1}{\sqrt{1+4\hat{z}^2}}$ tends to 0 as $\hat{z}$ tends to infinity. We can therefore approximate the $\tan^{-1} x$ terms using their MacLaurin expansion, which gives:

$$E_{r,\text{ square}} = \frac{4\Phi_t}{\pi w_t^2}\left[\frac{1}{\sqrt{1+4\hat{z}^2}^2} - \frac{1}{\sqrt{1+4\hat{z}^2}^4}\right] + o\left(\frac{1}{\hat{z}^4}\right), \tag{61}$$

In the case of the circular source, we can see that $\pi(\frac{2\hat{z}}{\pi\hat{z}^2-1})^2$ tends to 0 as $\hat{z}$ tends to infinity. We can therefore approximate the $(1+\pi(\frac{2\hat{z}}{\pi\hat{z}^2-1})^2)^{-1/2}$ term using its MacLaurin expansion, which gives:

$$E_{r,\text{ circ}} = \frac{\Phi_t}{2w_t^2}\left[\frac{2\pi\hat{z}^2}{\left(\pi\hat{z}^2-1\right)^2} + \frac{16\pi^2\hat{z}^4}{\left(\pi\hat{z}^2-1\right)^4}\right] + o\left(\frac{1}{\hat{z}^4}\right) \tag{62}$$

Therefore, the ratio $\frac{E_{r,\text{ point}}}{E_{r,\text{ square}}}$ can be approximated using (58) and (61) by:

$$\frac{E_{r,\text{ point}}}{E_{r,\text{ square}}} \sim \frac{1}{1-\frac{1}{4\hat{z}^4}} \underset{\hat{z}\to\pm\infty}{\longrightarrow} 1, \tag{63}$$

which proves (56).

On the other hand, the ratio $\frac{E_{r,\text{ point}}}{E_{r,\text{ circ}}}$ can be approximated using (58) and (62) by:

$$\frac{E_{r,\text{ point}}}{E_{r,\text{ circ}}} \sim \frac{1}{1+\frac{8}{\pi\hat{z}^2}} \underset{\hat{z}\to\pm\infty}{\longrightarrow} 1, \tag{64}$$

which proves (57). ■

TABLE 1. Link parameters for a single light source.

Parameter	Value
Room size	5×5×3 m
Coordinate system origin	Center of the ceiling
$\mathbf{u}_x$ and $\mathbf{u}_y$ axis	Contained in the ceiling plane
$\mathbf{u}_z$ axis	Points out of the room
Source position	$[0, 0, 0]$
Source type	Lambertian ($m_t = 1$)
Source area	3600 cm^2
Rectangular source size ($w_t \times h_t$)	600×600 mm
Source radiant flux (Φ_t)	1 W
Source normal vector ($\mathbf{n}_t$)	[0,0,-1]
Receiver dimensions ($p_r \times q_r$)	4.8×5.5 mm
Receiver normal vector ($\mathbf{n}_r$)	[0,0,1]
Receiver sensitivity (R_r)	1 A/W
Receiver FOV (Ψ_r)	90°

C. STUDY OF THE RECTANGULAR LIGHT SOURCE MODEL

We now focus on the near-field study of the models, starting with the rectangular-source model. Unlike point or circular transmitters, rectangular transmitters do not have any rotation symmetry. Therefore, we focus first on the study of this particularity. We consider here a rectangular light source of dimensions 600 × 600 mm, i.e., of area 3600 cm^2, and radiant flux $\Phi_t = 1$ W, placed at the center of a 5 × 5 m ceiling without tilt. We set the coordinate system origin at the center of the ceiling, which corresponds to the center of the transmitter, and the coordinate system axis is oriented as in Fig. 4(a). The receiver is not tilted either and has dimensions 4.8 × 5.5 mm with FOV 90° and sensitivity 1 A/W. These parameters are summed up in Table 1.

We set the receiver plane at $z = -10$ cm from the transmitter and compute the radiant flux received along the $\mathbf{u}_x$ axis on the one hand (y = 0 in (20)), and the diagonal of the source, on the other hand ($y = x$ in (20)). The results are represented in Fig. 7 and show that the radiant flux collected when moving along the diagonal is more significant than when moving along the $\mathbf{u}_x$ axis. This result comes from the fact that when moving along the diagonal, the receiver is directly exposed to more differential elements of transmitter over a longer distance than when moving along $\mathbf{u}_x$ axis because the diagonal length is longer than the half-side length.

This phenomenon tends to decrease when the vertical distance z between the transmitter and the receiver increases. For example, at 50 cm, the maximum difference of radiant flux is only 0.2 μW, whereas it is around 20 μW at 10 cm.

D. MODELS COMPARISON FOR NON-TILTED SOURCES AND RECEIVER

We compare now the rectangular and circular extended-source models with the point-source model. The parameters for the link geometry and the three kinds of transmitters are listed in Table 1. This means that the circular transmitter has the same area as the square transmitter, i.e., 3600 cm^2, which corresponds to a diameter of 677 mm. Consequently, both the square and circular sources have the same radiance

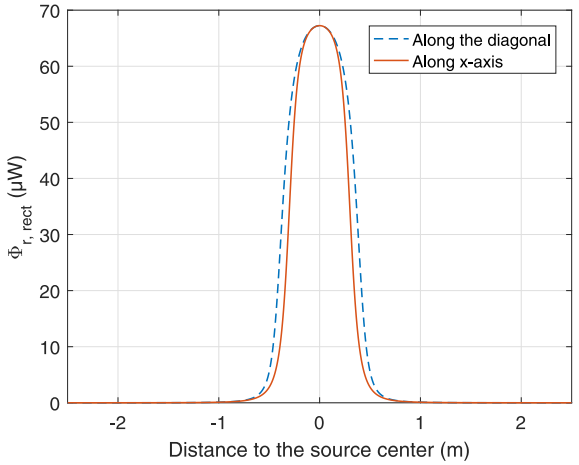

FIGURE 7. Evolution of the radiant flux collected by a non-tilted 4.8×5.5 mm receiver from a 1 W square source at 10 cm along the side direction and the diagonal direction.

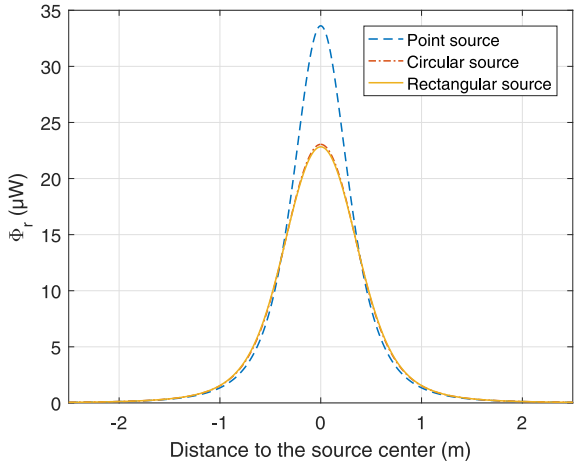

(a) z = -0.5 m

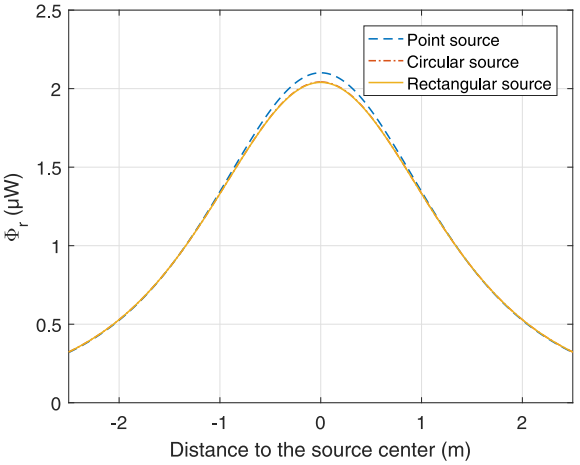

(b) z = -2 m

FIGURE 8. Evolution of the radiant flux collected by a non-tilted 4.8×5.5 mm receiver with different sorts of non-tilted 1 W sources at (a) 50 cm and (b) 2 m.

L_t, equal to 0.8842 W.m^{-2}. Fig. 8(a) shows the radiant flux collected by the receiver at $z = -0.5$ m from the three sorts of sources when it is moved along the line $x = y$, i.e., along the diagonal of the square transmitter. Fig. 8(b) then shows the same results at $z = -2$ m.

It appears clearly that the point-source model tends to overestimate the radiant flux collected, especially around the center of the transmitter. On the contrary, the radiant flux collected from the rectangular and circular extended sources tends to be more significant when moving away from the center of the transmitter (e.g., from $\pm$ 0.4 m in Fig. 8(a)). These results can be explained by the fact that, although both the extended and point sources emit the same average radiant flux Φ_t, this power will be more diffused in the case of the extended sources because their surfaces are larger than the point source. It leads to a reduced peak radiant flux collected but larger values on the sides of the transmitter.

Fig. 8 also clearly shows that the difference in radiant flux between the point and extended-source models reduces with the vertical distance z between the transmitter and the receiver. Fig. 9(a) further highlights this behavior by showing the evolution of the difference in the maximum radiant flux collected $\Delta\Phi_{r,\,\max}$ between the point source and the rectangular source on the one hand, and the point source and the circular source on the other hand. Therefore, in the case of a rectangular source, we have $\Delta\Phi_{r,\,\max} = \Phi_{r,\,\text{point (max)}} - \Phi_{r,\,\text{rect (max)}}$, with $\Phi_{r,\,\text{point (max)}}$ the maximum radiant flux collected with the point-source model, and $\Phi_{r,\,\text{rect (max)}}$ the maximum radiant flux collected with the rectangular extended-source model. In the case of a circular source, we have $\Delta\Phi_{r,\,\max} = \Phi_{r,\,\text{point (max)}} - \Phi_{r,\,\text{circ (max)}}$, with $\Phi_{r,\,\text{rect (max)}}$ the maximum radiant flux collected with the circular extended-source model. In practice, these maximums are reached in the transmitter's axis of reference, i.e., at the point of coordinates $(0, 0, z)$. We can see that in the case of a 3600 cm^2 rectangular source (blue-solid line), $\Delta\Phi_{r,\,\max}$ reaches 10.97 dBm at 10 cm but then quickly decreases to reach 1.68 dBm at 50 cm, 0.49 dBm at 1 m and 0.06 dBm at 3 m.

Fig. 9(a) also shows that this behavior is strongly mitigated as the transmitter dimensions decrease. At 10 cm, $\Delta\Phi_{r,\,\max}$ goes from 10.97 dBm for a 3600 cm^2 rectangular source down to 1.24 dBm with 100 cm^2, 14×10^{-3} dBm with 1 cm^2 and 0.14×10^{-3} dBm with 0.01 cm^2. These results show, on the one hand, the good accordance of the proposed model for extended rectangular sources with the point-source model when the transmitter dimensions are small and, on the other hand, that the point-source model is indeed relevant when considering most standard LED chips, especially infrared LED.

In addition, we can notice on Fig. 9(a) that whatever the surface considered, the $\Delta\Phi_{r,\,\max}$ curves have the same overall shape with the rectangular-source model as with the circular-source model, but that they have slightly lower values in the second case. This means the point-source model provides results closer to the circular-source model than to

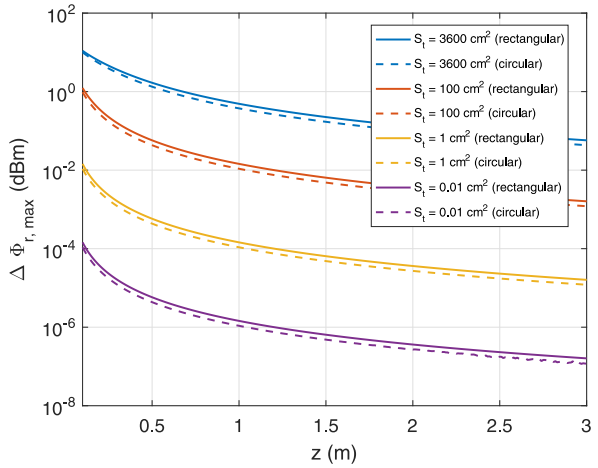

(a) $\Phi_{r,\,\text{point (max)}} - \Phi_{r,\,\text{rect (max)}}$ and $\Phi_{r,\,\text{point (max)}} - \Phi_{r,\,\text{circ (max)}}$.

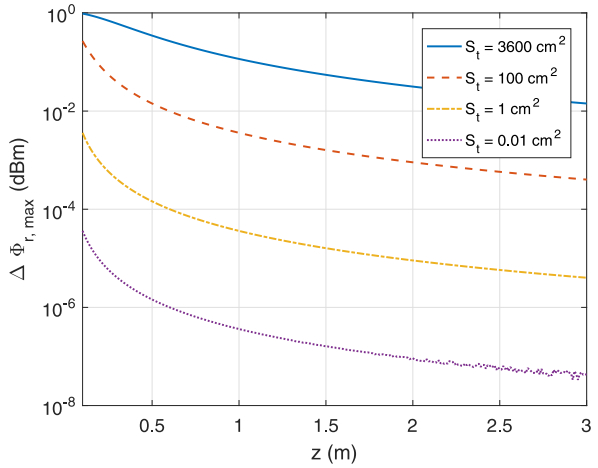

(b) $\Phi_{r,\,\text{circ (max)}} - \Phi_{r,\,\text{rect (max)}}$

FIGURE 9. Evolution of the difference of radiant flux collected with the vertical distance z and for different light source models and dimensions.

the rectangular-source model. Such a result is in line with Fig. 8, which shows that the radiant flux collected from the circular source is slightly larger than that from the rectangular source, even though both transmitters have the same surface area.

This difference is further highlighted by Fig. 9(b), which shows the difference in the maximum radiant flux $\Phi_{r,\,\text{rect (max)}}$ and $\Phi_{r,\,\text{circ (max)}}$ collected from, respectively, the rectangular transmitter and the circular light source. We notice that at 10 cm, for sources of 3600 cm^2 surface, which corresponds to a 600×600 mm rectangular source and a 677 mm diameter circular transmitter, there is a non-negligible 0.96 dBm difference; even if both transmitters have the same area, the distance between their contour and their center varies differently. In the circular-source case, this distance is equal to the source radius r_t, that is 33.85 cm. In the rectangular-source case, this distance varies from 30 cm at the half-width and half-length points to 42.43 cm at the corner points. The radiant flux received from the points around the corners of the rectangular source is thus more attenuated

TABLE 2. Link parameters for multiple tilted light sources.

Parameter	Value
Number of rectangular sources	2
Rectangular sources positions	$[-1.75, 1.75, 0]$, $[1.75, -1.75, 0]$
Number of circular sources	2
Circular sources positions	$[-1.75, -1.75, 0]$, $[1.75, 1.75, 0]$
Sources normal vectors ($\mathbf{n}_{t,j}$)	$[\pm 1/2, \pm 1/2, -\sqrt{2}/2]$
Receiver normal vector ($\mathbf{n}_r$)	[0,0,1]

because the distance to the receiver is larger, which results in an overall slightly lower radiant flux. However, as shown in Fig. 9(b), the difference reduces with the vertical distance to reach, still in the case of 3600 cm^2 sources, 0.01 dBm at 3 m. In parallel, we note that this difference also logically reduces with the transmitter area.

E. TILTED LIGHT SOURCES AND RECEIVER

We now consider the case of four light sources, two rectangular transmitters and two circular transmitters, deployed in a room as detailed in Table 2. Each transmitter is pointing toward the room's center and has an angle of 45° between its normal and $-\mathbf{u}_z$. On the other hand, the receiver is not tilted at first and is pointing toward the ceiling. The rest of the parameters are as in Table 1.

In such a case, we can apply the results detailed in Section IV. Fig. 10(a) shows the radiant flux distribution obtained with the rectangular and circular extended-source models. Each transmitter can be identified as the distribution presents four peaks. Note that each peak is logically not located at the exact $[x, y]$ positions of the transmitters because of their respective tilt angles.

Fig. 10(b) then represents the spatial distribution of the difference $\Delta\Phi_{r,\,\text{total}} = \Phi_{r,\,\text{point}} - \Phi_{r,\,\text{ext}}$ between the radiant flux distribution $\Phi_{r,\,\text{point}}$ obtained with the point-source model and that obtained with the rectangular and circular extended-source models $\Phi_{r,\,\text{ext}}$. It shows that this difference fluctuates between ± 0.07 dBm. Note that if the transmitter dimensions are reduced to 1×1 mm, then $\Delta\Phi_{r,\,\text{total}}$ is in the order of 10^{-7} dBm. These results confirm that the point-source model remains a good approximation even for large sources if the link distance is large enough.

The same simulations can be efficiently run with a tilted receiver. For example, Fig. 11 represents the radiant flux distribution obtained with the rectangular and circular extended-source models when the receiver is tilted by 30° around $\mathbf{u}_y$ axis, so that its normal vector is $\mathbf{n}_r = [-\sqrt{3}/2, 0, 1/2]$. This distribution exhibits a cutting line around $x = 0.6$ m, which is because for x values lower than this threshold, the receiver cannot receive the light beams coming from the right light sources because of its tilt. Finally, note that the radiant flux difference $\Delta\Phi_{r,\,\text{total}}$, although not represented, still fluctuates between -0.28 and 0.08 dBm.

VI. EXPERIMENTAL VERIFICATION OF THE PROPOSED CIRCULAR-SOURCE MODEL

In order to verify the relevance of the proposed circular-source model, we finally compare the theoretical received

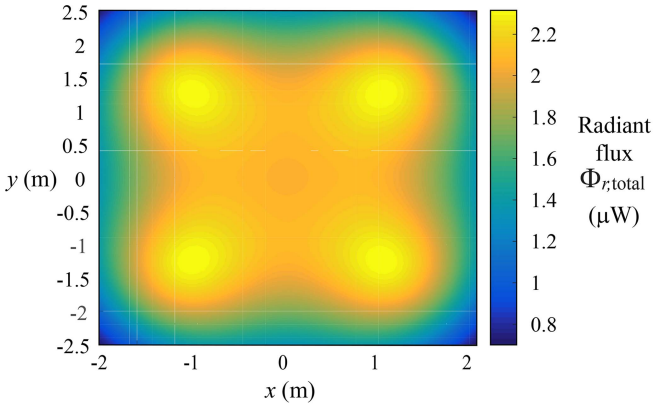

(a) Total radiant flux distribution $\Phi_{r;\text{total}}$ (μW).

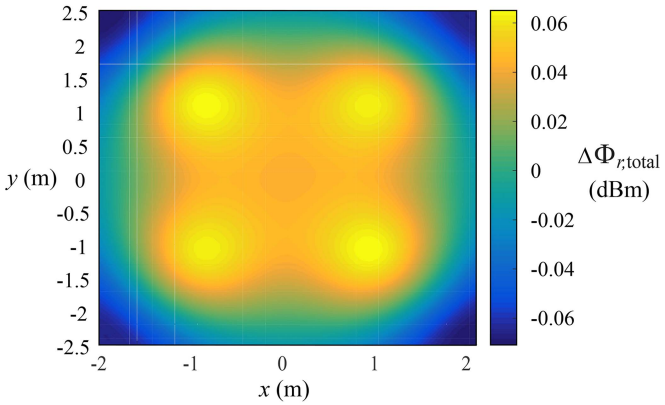

(b) Difference of radiant flux $\Delta\Phi_{r;\text{total}}$ (dBm).

FIGURE 10. Distribution, in the case of four light sources, of (a) the radiant flux received using the rectangular and circular extended-source models and (b) the difference $\Delta\Phi_{r,\text{ total}} = \Phi_{r,\text{ point}} - \Phi_{r,\text{ ext}}$ of radiant flux compared to the point-source model.

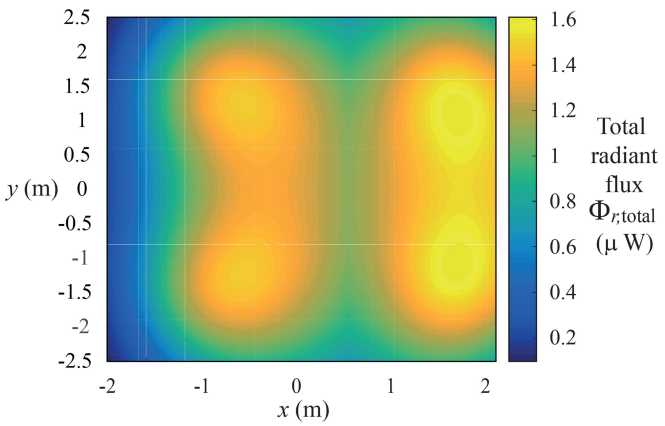

FIGURE 11. Radiant flux distribution in the case of a tilted receiver with normal vector $\mathbf{n}_r = [-\sqrt{(3)}/2, 0, 1/2]$.

radiant flux $\Phi_{r,\text{ circ}}$ given by (33) with actual measurements. For this experiment, we use a circular LED lamp of diameter 135 mm with a diffuser. It is assumed from the manufacturer's description that the resulting emission pattern is Lambertian with an order 1. The nameplate of the lamp states that the maximum electrical power is 12 W. However,

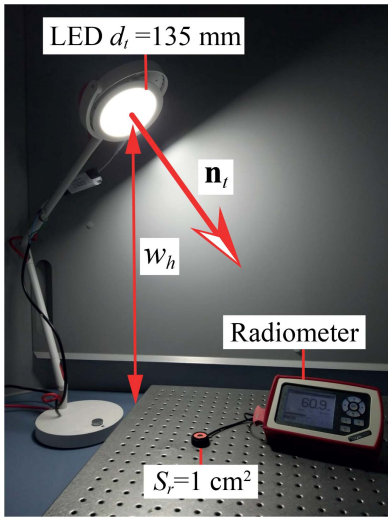

FIGURE 12. Experimental setup used to verify the radiant flux model proposed for a circular extended source.

the actual electrical power dissipated from the lamp and its regulated DC source is 7.04 W, whereas the measured electrical power consumed by the source itself is 6.05 W. These values were obtained with a Hopi HP9800 Wattmeter and correspond to an emitted radiant flux $\Phi_t = 1267$ mW. The resulting luminous efficiency of the lamp is thus 20.94%.

The radiant flux is measured with a Thorlabs PM100D digital radiometer connected to a 400-1100 nm broadband S121C detector (receiver). The instrument was calibrated to measure the radiant flux in a dark room with a controlled temperature of 23°C. A Cartesian coordinate system with a total working area of 588×588 mm is created by placing the center of the LED at the vertex of the second quadrant. The light source is placed on a swivel mount with an associated unit normal vector $n_t = [0.195743; -0.0616514; -0.978715]$ so that it is titled. In addition, it is placed at a vertical working distance (height) $z = -63.5$ cm. Fig. 12 shows the corresponding experimental setup.

The radiant flux is measured at each point of a 22 columns (x-axis) by 21 rows (y-axis) grid, with columns and rows spacing of 25.4 mm. Therefore, the total number of sampling points J is 462. The resulting radiant flux distribution $\Phi_{r,\text{ exp}}$ is represented in Fig. 13(a), whereas the corresponding theoretical radiant flux distribution $\Phi_{r,\text{ circ}}$ is represented in Fig. 13(b). The difference between both distribution is computed and represented in Fig. 13(c), which shows this difference fluctuates between $+2$ μW and -4 μW.

In order to better compare the measured radiant flux distribution with the theoretical one, we define the following correlation coefficient c_c:

$$c_c = \sqrt{1 - \frac{\sum_{j=1}^{J} \left(\Phi_{r,\text{ circ}}(x_j, y_j) - \Phi_{r,\text{ exp}}(x_j, y_j)\right)^2}{\sum_{j=1}^{J} \Phi_{r,\text{ circ}}^2(x_j, y_j) - \frac{1}{J}\left(\sum_{j=1}^{J} \Phi_{r,\text{ circ}}(x_j, y_j)\right)^2}}, \tag{65}$$

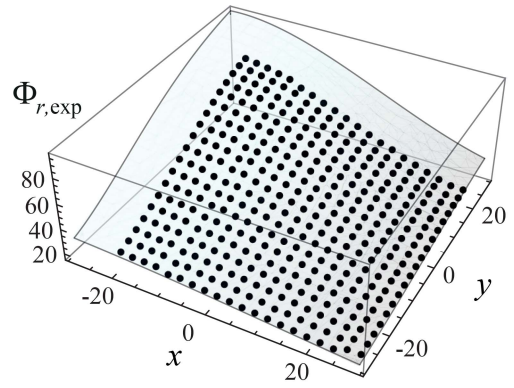

(a) Radiant flux distribution measured $\Phi_{r,\,\mathrm{exp}}$ in μW.

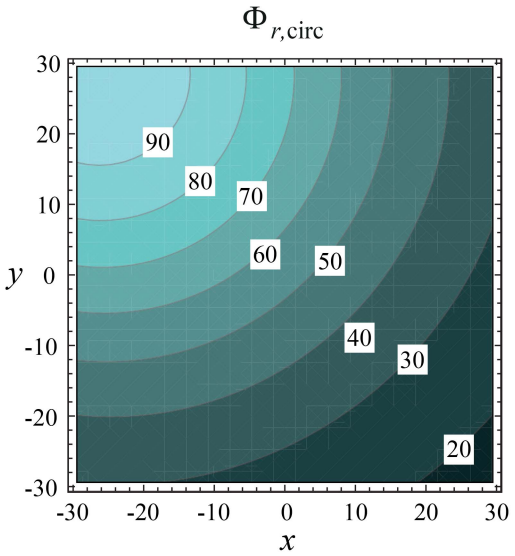

(b) Theoretical radiant flux distribution $\Phi_{r,\,\mathrm{circ}}$ in μW.

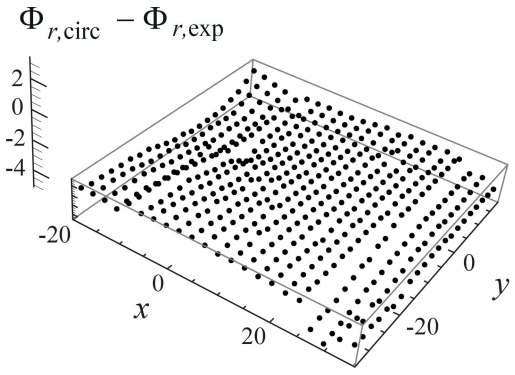

(c) Radiant flux error $\Phi_{r,\,\mathrm{circ}} - \Phi_{r,\,\mathrm{exp}}$ in μW.

FIGURE 13. Comparison between the radiant flux distribution measured $\Phi_{r,\,\mathrm{exp}}$ and the theoretical distribution $\Phi_{r,\,\mathrm{circ}}$.

with (x_j, y_j) be the j-th sampling point, $\Phi_{r,\,\mathrm{exp}}(x_j, y_j)$ the radiant flux measured at this point and $\Phi_{r,\,\mathrm{circ}}(x_j, y_j)$ the theoretical radiant flux at this point. In the configuration just described, we find that $c_c = 0.995508$. We can therefore conclude that the radiant flux model for an extended circular source with tilt we propose in this paper gives a very accurate estimate of the real radiant flux collected for such a source.

TABLE 3. Table of notations.

Notation	Definition
$\bullet$	Vector dot product
$\times$	Vector cross product
$\|\|.\|\|$	Vector norm
$\mathbf{F}$	Parametric vector function
O	Cartesian coordinate origin
r	Receiver index
t	Transmitter index
$\mathbf{v}$	Vector
$\mathbf{v'}$	Rotated vector
x	Scalar variable

VII. CONCLUSION AND FUTURE WORKS

This paper presents a model of the irradiance of one or several extended and tilted light sources at the level of a tilted photoreceiver. In particular, it details the irradiance distribution produced by rectangular and circular sources, and then shows in the latter case the good accordance between the theoretical distribution and actual measurements. These models then allow deducing the radiant flux collected by the receiver easily, and can thus be used to establish channel link budgets when large-area light sources are used as OWC transmitters, as is sometimes the case in VLC with LED panels or wide-area OLEDs.

The extended-source model proposed here can also be seen as an extension of the already widely used point-source model, as the results obtained with the former in the case of small-area sources are consistent with those obtained with the latter. Therefore, it can be used in the same way in LOS and NLOS channel simulations with the code provided as supplementary material.

The results we show here, however, only concern the case of Lambertian rectangular and circular sources. Therefore, our future work will focus on the case of transmitters with different shapes, such as half-circle or polygonal sources, but also on non-Lambertian sources, starting with sources with an emission pattern following a generalized Lambertian cosine law with $m_t > 1$. In addition, an accurate modeling of the responsivity of photoreceivers will be proposed to better capture their angular dependance and go beyond the concept of binary FOV used in usual models.

APPENDIX A
LIST OF NOTATIONS

Tables 3 and 4 sum up respectively the various notations and variables used throughout the paper.

APPENDIX B
HOW TO USE THE MODELS PROPOSED

This paper proposes two models for the radiant flux collected by a photoreceiver from either an extended rectangular light source or an extended circular source. These models can be used instead of the usual point-source model reminded in

TABLE 4. Table of variables.

Variable	Definition
A, B, C, D	Buffer variables
a_r, b_r, c_r	Receiver director cosines
A_r, B_r, C_r	Rotated receiver director cosines
a_t, b_t, c_t	Transmitter director cosines
c_c	Correlation coefficient
C_t	Transmitter contour
ds_r	Receiver differential element of area
ds_t	Transmitter differential element of area
d_t	Circular transmitter diameter
$d_{t,r}$	Distance between the transmitter and the point at which the irradiance is calculated
E_r	Received irradiance (general case)
$E_{r,\,\text{circ}}$	Received irradiance (circular source)
$E_{r,\,\text{point}}$	Received irradiance (point source)
$E_{r,\,\text{rect}}$	Received irradiance (rectangular source)
$E_{r,\,\text{square}}$	Received irradiance (square source)
$H(0)$	LOS channel DC gain
I_t	Transmitter intensity
J	Total number of sampling points
$\mathbf{k}$	Unit vector as rotation pivot
L_t	Transmitter radiance
m_t	Transmitter Lambertian order
N_r	Noise power
$\mathbf{n}_r$	Receiver normal unit vector associated with ds_r
$\mathbf{n}_t$	Transmitter normal unit vector associated with ds_t
O_t	Transmitter Cartesian coordinate system
P, Q, R	Parametric functions
$\mathbf{p}_r$	Receiver vector position
$\mathbf{p}_t$	Transmitter vector position
R_r	Receiver responsivity
r_t	Transmitter radius
R_t	Transmitter radiation pattern
S_r	Receiver sensitive surface
S_t	Transmitter surface
T	Total number of transmitters
$\mathbf{u}_x, \mathbf{u}_y, \mathbf{u}_z$	Cartesian coordinate unit vectors
$\mathbf{u}_X, \mathbf{u}_Y, \mathbf{u}_Z$	Rotated Cartesian coordinate unit vectors
$\mathbf{v}_{t,r}$	Unit vector between ds_t and ds_r
w_t and h_t	Rectangular transmitter dimensions
x, y, z	Cartesian coordinates
X, Y, Z	Rotated Cartesian coordinates
x_j, y_j	Sampling point coordinates
x_t, y_t, z_t	Transmitter coordinates
$\tilde{z}$	Normalized axial coordinate
$\alpha_t, \beta_t, \gamma_t$	Transmitter Euler angles
$\Delta\Phi_{r,\,\text{max}}$	Difference of maximum radiant flux received between two models (single source)
$\Delta\Phi_{r,\,\text{total}}$	Difference of maximum radiant flux received between two models (multiple sources)
$\delta\Sigma$	Closed contour
θ_t	Transmitter polar angle
$\tilde{\rho}$	Normalized radial coordinate
Σ	Closed surface
Φ_r	Radiant flux received (general case)
$\Phi_{r,\,\text{circ}}$	Radiant flux received (circular source)
$\Phi_{r,\,\text{circ (max)}}$	Maximum radiant flux on a receiver (circular source)
$\Phi_{r,\,\text{exp}}$	Radiant flux measured
$\Phi_{r,\,\text{ext}}$	Radiant flux received (extended source)
$\Phi_{r,\,\text{point}}$	Radiant flux received (point source)
$\Phi_{r,\,\text{point (max)}}$	Maximum radiant flux on a receiver (point source)
$\Phi_{r,\,\text{rect}}$	Radiant flux received (rectangular source)
$\Phi_{r,\,\text{rect (max)}}$	Maximum radiant flux on a receiver (rectangular source)
$\Phi_{r,\,\text{total}}$	Total radiant flux on a receiver (multiple sources)
ϕ_t	Transmitter azimuth angle
Φ_t	Transmitter average radiant flux
$\Phi_{t,1/2}$	Transmitter semi-angle at half power
χ	Rotation angle
ψ_r	Receiver incidence angle
Ψ_r	Receiver field-of-view
ω_t	Transmitter polar angle

Section II to calculate the link budget available in a given set up and then design an OWC system accordingly. For example, Fig. 1 shows the example of a set up where square lighting panels are used to cover a whole room with a LiFi access to user equipped with handled devices like mobile phones. In such a case, the distance between the light sources and the photoreceiver might be rather short depending on the movement of the users so that the proposed radiant flux models can prove useful. In order to use them, the next steps can be followed:

1) Define the geometry of the room in which the OWC system is to be deployed and set a Cartesian coordinate system.
2) Define the radiometric and geometrical properties of the light source (radiant exitance, circular or rectangular shape, area, tilt angle$\cdots$).
3) Define the properties of the photoreceiver (location, size, responsivity, tilt angle$\cdots$).
4) Compute the LOS radiant flux collected by the photoreceiver from the received irradiance given by (20) in the case of a rectangular source or by (26) in the case of a circular source, including the change of variables given by (34) and (35) if the source is titled.
5) Repeat the operation for any source used and then add the resulting radiant flux to obtain the total radiant flux collected using (43).
6) NLOS contributions can also be added by following the methods described in [9] (deterministic method) or [11] (stochastic method) and replacing the point-source model by the extended-source model needed.
7) The resulting LOS and NLOS contributions can then be added to obtain the total radiant flux collected by the photoreceiver and then deduce, using (1), the optical SNR of the OWC link. This optical SNR can then be linked to the electrical SNR and the bit-error rate of the link depending on the modulation used.

REFERENCES

[1] F. R. Gfeller and U. Bapst, "Wireless in-house data communication via diffuse infrared radiation," *Proc. IEEE*, vol. 67, no. 11, pp. 1474–1486, Nov. 1979.

[2] J. M. Kahn and J. R. Barry, "Wireless infrared communications," *Proc. IEEE*, vol. 85, no. 2, pp. 265–298, Feb. 1997.

[3] M. A. Khalighi and M. Uysal, "Survey on free space optical communication: A communication theory perspective," *IEEE Commun. Surveys Tuts.*, vol. 16, no. 4, pp. 2231–2258, 4th Quart., 2014.

[4] N. Saha, M. S. Ifthekhar, N. T. Le, and Y. M. Jang, "Survey on optical camera communications: Challenges and opportunities," *IET Optoelectron.*, vol. 9, no. 5, pp. 172–183, Oct. 2015.

[5] Y. Tanaka, T. Komine, S. Haruyama, and M. Nakagawa, "Indoor visible communication utilizing plural white LEDs as lighting," in *Proc. 12th IEEE Int. Symp. Pers. Indoor Mobile Radio Commun. (PIMRC)*, vol. 2. San Diego, CA, USA, Oct. 2001, pp. F81–F85.

[6] T. Komine and M. Nakagawa, "Fundamental analysis for visible-light communication system using LED lights," *IEEE Trans. Consum. Electron.*, vol. 50, no. 1, pp. 100–107, Feb. 2004.

[7] H. Haas, L. Yin, Y. Wang, and C. Chen, "What is LiFi?" *J. Lightw. Technol.*, vol. 34, no. 6, pp. 1533–1544, Mar. 15, 2016.

[8] S. Dimitroc and H. Haas, *Principles of LED Light Communications: Towards Networked Li-Fi*. Cambridge, U.K.: Cambridge Univ. Press, 2015.

[9] Z. Ghassemlooy, W. Popoola, and S. Rajbhandari, *Optical Wireless Communications: System and Channel Modeling With MATLAB*. Boca Raton, FL, USA: CRC Press, 2012.

[10] S. Arnon, J. Barry, G. Karagiannidis, R. Schober, and M. Uysal, *Advanced Optical Wireless Communication Systems*. New York, NY, USA: Cambridge Univ. Press, 2012.
[11] R. Pérez-Jiménez, J. Berges, and M. J. Betancor, "Statistical model for the impulse response on infrared indoor diffuse channels," *Electron. Lett.*, vol. 33, no. 15, pp. 1298–1300, Jul. 1997.
[12] F. J. López-Hernández, R. Pérez-Jiménez, and A. Santamaría, "Ray-tracing algorithms for fast calculation of the channel impulse response on diffuse IR wireless indoor channels," *J. Opt. Eng.*, vol. 39, no. 10, pp. 2775–2780, Oct. 2000.
[13] V. Pohl, V. Jungnickel, and C. von Helmolt, "Integrating-sphere diffuser for wireless infrared communication," *IEE Proc. Optoelectron.*, vol. 147, no. 4, pp. 281–285, Aug. 2000.
[14] I. Moreno, "LED irradiance pattern at short distances," *Appl. Opt.*, vol. 59, no. 1, pp. 190–195, Jan. 2020.
[15] *The International System of units, Appendix 2: Mise en Pratique for the definition of the Candela and Associated Derived Units for Photometric and Radiometric Quantities in the SI*, 9th ed., BIPM, Saint-Cloud, France, 2019.
[16] A. A. Gaertner, "Optical radiation measurement," in *Modern Metrology Concerns*. Rijeka, Croatia: IntechOpen, 2012, ch. 9.
[17] J. M. Palmer, "Getting intense on intensity," *Metrologia*, vol. 30, no. 4, pp. 371–372, Jan. 1993.
[18] D. Wu *et al.*, "Effect of optimal Lambertian order for cellular indoor optical wireless communication and positioning systems," *Opt. Eng.*, vol. 55, no. 6, Jun. 2016, Art. no. 066114.
[19] J. M. Palmer, and B. G. Grant, *The Art of Radiometry*. Bellingham, WA, USA: SPIE Press, 2010.
[20] J. R. Howell, R. Siegel, and M. P. Mengüç, "Configuration factors for diffuse surfaces with uniform radiosity," in *Thermal Radiation Heat Transfer*. New York, NY, USA: CRC Press, 2010, pp. 151–204.
[21] I. N. Bronshtein, K. A. Semendyayev, G. Musiol, and H. Mühlig, *Handbook of Mathematics, 4th ed*. Berlin, Germany: Springer-Verlag, 2004.

JUAN CAMILO VALENCIA-ESTRADA received the M.Sc. degree in applied mathematics from Universidad EAFIT, Medellín, Colombia, in 2010, and the Ph.D degree in optics from Centro de Investigaciones en Optica, Leon, National Council for Science and Technology, Mexico, in 2015. He has been a Production Engineer with Universidad EAFIT since 1987. He is currently a Senior Researcher with Oledcomm. He has published 15 peer-review articles and has filed seven patents. He has significant experience in mechanical and optomechanical design and manufacture. His past and current research cover optical design, optical links antennae, and optical wireless communications.

BASTIEN BÉCHADERGUE received the Engineering degree from ISAE-Supaero, Toulouse, France, the M.S. degree in communication and signal processing from Imperial College London, London, U.K., in 2014, and the Ph.D. degree in signal and image processing from the UVSQ, University Paris–Saclay, France, in 2017, for his work on visible light communication and range-finding for automotive applications. He is currently in charge of the research activities with Oledcomm, a company specialized in optical wireless communication product development. His current research interests thus include optical wireless communications and especially LiFi but also optical positioning.

JORGE GARCÍA-MÁRQUEZ received the Electronics Engineering degree from Universidad Iberoamericana, León, Mexico, in 1994, the M.Sc. and Ph.D. degrees in optics from the Universidad de Guanajuato, Mexico, in 1995 and 1998, respectively, and the Habilitation degree (Doctor in Sciences) in photonics from the Université de Versailles Saint-Quentin, France, in 2013. He was a Researcher with the Centro de Investigaciones en Optica from 1999 to 2013, le Cnam until December 2014, then a Senior Researcher with Oledcomm until 2019. He has published 35 peer-review articles and has filed 13 patents. He is currently with Laboratoire National de Métrologie et d'Essais. His past and current research cover length measurements, phase recovery, optical super-resolution, optical links antennae, optical wireless communications, and Lidars.